Lab on a Chip

Accepted Manuscript

This article can be cited before page numbers have been issued, to do this please use: F. Tian, W. Zhang, L. Cai, S. Li, G. Hu, Y. Cong, C. Liu, T. Li and J. Sun, *Lab Chip*, 2017, DOI: 10.1039/C7LC00671C.

This is an Accepted Manuscript, which has been through the Royal Society of Chemistry peer review process and has been accepted for publication.

Accepted Manuscripts are published online shortly after acceptance, before technical editing, formatting and proof reading. Using this free service, authors can make their results available to the community, in citable form, before we publish the edited article. We will replace this Accepted Manuscript with the edited and formatted Advance Article as soon as it is available.

You can find more information about Accepted Manuscripts in the author guidelines.

Please note that technical editing may introduce minor changes to the text and/or graphics, which may alter content. The journal's standard Terms & Conditions and the ethical guidelines, outlined in our author and reviewer resource centre, still apply. In no event shall the Royal Society of Chemistry be held responsible for any errors or omissions in this Accepted Manuscript or any consequences arising from the use of any information it contains.

ROYAL SOCIETY OF CHEMISTRY

rsc.li/loc

View Article Online
DOI: 10.1039/C7LC00671C

Microfluidic Co-flow of Newtonian and Viscoelastic Fluids for High-resolution Separation of Microparticles

Fei Tian,[1,2] Wei Zhang,[2,5] Lili Cai,[3] Shanshan Li,[1] Guoqing Hu,[4,5] Yulong Cong,[3] Chao Liu,[2,5] ⋆ Tiejun Li[1⋆] and Jiashu Sun[2,5⋆]

[1]School of Mechanical Engineering, Hebei University of Technology, Tianjin 300401, China

[2]CAS Key Laboratory of Standardization and Measurement for Nanotechnology, CAS Center for Excellence in Nanoscience, National Center for Nanoscience and Technology, Beijing 100190, China

[3]Department of Geriatric Laboratory Medicine, Chinese PLA General Hospital, Beijing 100853, China

[4]State Key Laboratory of Nonlinear Mechanics, Institute of Mechanics, Chinese Academy of Sciences, Beijing 100190, China

[5]University of Chinese Academy of Sciences, Beijing 100049, China

E-mail address: liuc@nanoctr.cn; li_tiejun@hebut.edu.cn; sunjs@nanoctr.cn

Tel:+86-10-82545621; Fax: +86-10-82545621

View Article Online
DOI: 10.1039/C7LC00671C

Abstract

The microfluidic passive control of microparticles largely relies on the hydrodynamic effects of the carrier media such as Newtonian fluids and viscoelastic fluids. Yet the viscoelastic/Newtonian interfacial effect has been scarcely investigated, especially for high-resolution particle separation. Here we report a microfluidic co-flow of Newtonian (water or PBS) and viscoelastic fluids (PEO) for size-dependent separation of microparticles. The co-flow condition generates a stable viscoelastic/Newtonian interface, giving rise to the wall-directed elastic lift forces that compete with the center-directed lift forces, and efficiently hinder the migration of microparticles from the Newtonian to viscoelastic fluids in a size-dependent manner. An almost complete separation of a binary mixture of 1 μm and 2 μm polystyrene particles is achieved by the co-flow of water and a very dilute PEO solution (100 ppm), whereas the sole use of water or PEO could not lead to an efficient separation. This co-flow microfluidic system is also applied for separation of *Staphylococcus aureus* (1 μm) from platelets (2-3 μm) with > 90 % efficiencies and purities.

View Article Online
DOI: 10.1039/C7LC00671C

Introduction

The precise separation of cells and microparticles for both preparative and analytical purposes is central to numerous applications in biology, clinical diagnosis, chemistry, and materials.[1-3] To date, the microfluidic passive control of microparticles largely relies on the hydrodynamic effects of the carrier medium, such as inertia[4] and viscoelasticity,[5] while enabling an effective particle/cell manipulation in label-free and external force field-free manners. The driving force for passive particle separation, such as inertial (F_L) or viscoelastic (F_e) lift force, is strongly dependent on the particle diameter a ($F_L \propto a^4$ or $F_e \propto a^3$).[5-7] Modulation of F_L or F_e allows for size-based separation of microparticles/cells with diameters from several to several tens of microns inside microchannels.

Inertial microfluidics with relatively high flow rates has been employed to manipulate microparticles in circular,[8, 9] square,[10, 11] and rectangular[12, 13] microchannels, in which sufficient inertial effects are emerged over the Reynolds numbers (*Re*) ranging from several tens to hundreds in Poiseuille flow ($Re = \rho U_{\max} D/\eta$, where ρ is the fluid density, $U_{\max}$ is the maximum flow velocity, D is the microchannel cross-section dimension, and η is the dynamic viscosity). Coupled with the secondary flows induced in structured[14-17] or curved[18-21] microchannels, inertial microfluidics has been intensively used for enrichment, separation, and stretching measurement of cells and microparticles. In comparison with inertial microfluidics generally using Newtonian fluids as the carrier medium, viscoelastic microfluidics relies on the elasticity by adding synthetic or biological polymers into the carrier medium. The elastic lift force assists in focusing particles along the centerline of a microchannel at moderate Weissenberg number ($Wi = \lambda\dot{\gamma}$, where λ is the fluid relaxation

View Article Online
DOI: 10.1039/C7LC00671C

time and $\dot{\gamma}$ is the shear rate), attributed to the non-uniform normal stress differences.[5, 22] With the merits of wide range of working flow rates[23, 24] and simple focusing pattern,[25, 26] viscoelastic microfluidics has been applied to the separation of a variety of cells, including circulating tumor cells (CTC),[27] red blood cells,[25, 28-30] bacteria,[30] and *etc*.

To improve the separation performance by inertial or viscoelastic microfluidics, sheath flow has been frequently implemented to pre-align the particles, before the particles laterally migrate in a size-dependent manner driven by inertial or elastic lift forces.[23, 25] Sheath flow of viscoelastic carrier medium has also been coupled with "pinched flow fractionation" mechanism for enhanced chromatographic particle separation.[31, 32] Most of these works use sheath and sample fluids with the same rheological property, where particle migration is not influenced by the sheath/sample interface. Recently, the co-flow of Newtonian (sheath) and viscoelastic (sample) fluids is developed to effectively transfer particles from the viscoelastic streams into the Newtonian streams for particle/cell washing and separation.[33, 34]

Despite their advantages and extensive applications, high-resolution separation of microparticles with relatively small and similar sizes, *e.g.* separation of a binary mixture of 1 μm and 2 μm particles, is still challenging in inertial or viscoelastic microfluidics, because the acting lift forces and focusing positions continuously vary with particle size. Several strategies have been developed to improve the sensitiveness of the focusing position with respect to particle size. Guan *et al*. design a spiral microchannel with a trapezoidal cross-section to sophisticatedly modify spatial distribution of inertial lift forces and secondary flow drag forces, generating a sharp transition of particle focusing position by

View Article Online
DOI: 10.1039/C7LC00671C

adjusting the size-dependent critical flow rate.[35] Our previous work demonstrates a off-center shifting of viscoelastic focusing position for particles with *a* larger than a critical value of 0.25-0.3*D* by engineering the distribution of compressive normal stress over the particle surface.[27] However, to apply these strategies to smaller microparticles around 1 μm in diameter inevitably use scaled-down microchannels, requiring more sophisticated fabrication and a lowered flow rate.

Here we report a microfluidic co-flow of Newtonian and viscoelastic fluids for size-dependent separation of microparticles smaller than 3 μm by utilizing the interfacial effect between these two types of fluids (Fig. 1). The elastic lift forces acting on the particle dramatically alter at the interface of two fluids due to the absence of the elastic stresses at the Newtonian side flow. We theoretically estimate the interfacial elastic lift forces and predict a size-selective penetration of particles across the interface. Through manipulation of this size-selective interface penetration, we can completely separate the mixture of polystyrene (PS) particles with diameters of 1 μm and 2 μm, and isolate *Staphylococcus aureus* (SA) from platelets with high efficiencies. Both the theoretical and experimental results show a larger separation distance between different size particles by the present method, compared with the methods based on pure Newtonian or pure viscoelastic flow. Our work thus provides a versatile, label-free, and high-resolution approach for efficient separation of small microparticles.

View Article Online
DOI: 10.1039/C7LC00671C

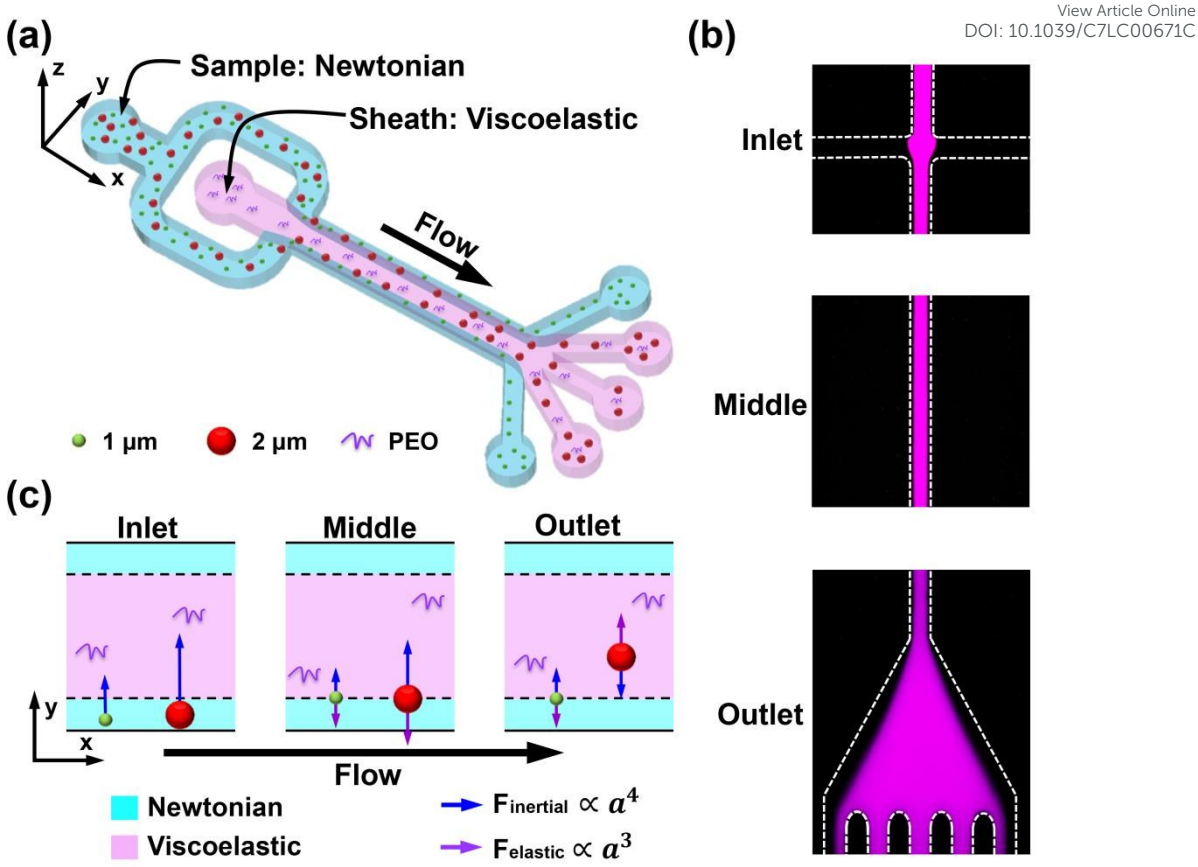

Fig. 1. (a) Schematic of the microfluidic device for particle separation using the co-flow of viscoelastic and Newtonian media. The microchannel consists of two inlets for sample fluid (Newtonian fluid) and sheath fluid (viscoelastic fluid), one straight separation channel with a rectangular cross-section (50 μm high and 20 μm wide), and five outlets for the collection of large and small particles. (b) Visualization of the interface between the sample (300 μL/h) and sheath (2400 μL/h) flows by spiking fluorescent nanoparticles (100 nm in diameter) into the sheath inlet. (c) A schematic mechanism of the size-based particle separation. Particles are initially aligned along the sidewalls by the sheath flow at the inlet and then pushed away from the sidewalls by the centerline-directed inertial lift forces. Small particles cannot traverse the interface between Newtonian and viscoelastic media due to the dominance of wall-directed interfacial elastic lift forces, whereas large particles cross the interface due to the dominated

View Article Online
DOI: 10.1039/C7LC00671C

inertial lift forces.

Materials and methods

Device design and fabrication

The microchannel with a uniform height (H) of 50 μm consists of two inlets for sheath and sample fluids, a straight separation section (width×length, $W \times L$, 20 μm×15 mm), and five outlets for small particles (two side outlets) and large particles (three center outlets) (Figs. 1a and S1). The microchannels were fabricated using the standard soft-lithography techniques with SU8-2050 master mold on a silicon substrate. The degassed poly(dimethylsiloxane) (PDMS) was cast over the mold and then baked in an oven at 80 ℃ for 2 h. The molded PDMS slab was bonded to a glass substrate (25 mm × 75 mm) post oxygen plasma treatment, followed by inserting the connection tubes into the inlet/outlet ports. The assembled device was finally placed into an oven at 70 ℃ for 30 min to enhance bonding.

Sample preparation

For polystyrene (PS) particle experiments, viscoelastic medium as the sheath flow was prepared by adding PEO (M_w = 600 KDa, Sigma-Aldrich, USA) powder to deionized (DI) water at various concentrations of 50, 100, 300, and 1200 part per million (ppm). The dissolution of PEO powder was accelerated by 1 h of gentle stirring (at <30 rpm) and was then prepared by swinging them gently for 24 h to secure good solutions. The suspensions of 1 μm and 2 μm PS particles (1 wt %, Thermo Fisher Scientific, USA) were diluted in the pre-determined solutions to 0.02 and 0.2 wt %, respectively. To prevent particle aggregation, surfactant Tween 20 (Sigma-Aldrich, USA) was added into the suspensions at 0.02 w/v %.

View Article Online
DOI: 10.1039/C7LC00671C

For cell experiments, the viscoelastic medium was prepared by adding the PEO powder to 1× phosphate buffered saline (PBS) to a final concentration of 100 ppm PEO. Platelets were obtained from the Chinese PLA General Hospital (Beijing, China) and stored by gently shaking at 22 ℃. Before use, the platelet sample was diluted 4 times with 1× PBS. SA was cultured in LB Broth (Sigma-Aldrich, USA) on a shaker at 37 ℃ for 12 h. Experiments involving platelets were performed in compliance with the hospital guidelines (The Ethics Guidelines for Research Involving Human Subjects or Human Tissue from the Chinese PLA General Hospital).

Experimental Procedures and Image Analysis

The sheath and sample fluids were separately injected into the microchannel using two syringe pumps (Pump 11 Elite, Harvard Apparatus, USA). The flow rates were precisely adjusted to pinch the sample fluid into narrow streams along the sidewalls. We used various sheath flow rates ranging from 1.2 to 3.0 mL/h with a fixed sample flow rate of 0.3 mL/h, leading to sheath/sample flow ratios of 4 to 10. The concentration of PEO as the sheath medium was 100 ppm. The particle trajectories were observed using an inverted microscope (Eclipse Ti, Nikon, Japan) with a 20× objective. The images and movies were recorded with a high-speed camera (Phantom v7.3, Vision Research Inc., USA) and Phantom Camera Control software. The images were processed with the ImageJ software package (NIH): the time-series images (1000 images) were stacked using *z*-projection with the “standard deviation” option. The particle distributions were determined by conducting automatic particle analysis for 100 images (≥1000 particles), and the cell distributions were manually analyzed for 100 images (≥1000 cells). The purity is defined as the number ratio of the

View Article Online
DOI: 10.1039/C7LC00671C

targeted to the total microparticles. The separation efficiency is defined as the percentage of microparticles of a certain size at the preferred outlet.

PEO solution properties

The relaxation times for the PEO solutions of M_w = 600 KDa at various concentrations were determined by the empirical formula based on capillary breakup extension rheometry (CaBER) measurement: $\lambda = 18\lambda_Z \left(c/c^*\right)^{0.65}$,[36] where the overlapping concentration c^* is expressed as $0.77/[\eta]$,[37] the intrinsic viscosity $[\eta]$ is given by the Mark-Houwink relation, $[\eta] = 0.072M_w^{0.65}$,[38] and the Zimm relaxation time λ_Z is determined as $\lambda_Z = F[\eta]M_w\eta_s/N_Ak_BT$ according to Zimm theory (here the pre-factor F is 0.463 for PEO solutions, the solvent viscosity η_s is $1\times10^{-3}\,Pa\cdot s$, and N_A and k_B represent the Avogadro's number and the Boltzmann's constant, respectively). The λ is consequently expressed as $0.128M_w^{2.07}\eta_s c^{0.65}/N_Ak_BT$, determining the relaxation times of 0.078, 0.123, 0.251, and 0.619 ms for the PEO concentrations of 50, 100, 300, and 1200 ppm, respectively. The polymeric contribution η_p to the viscosity of a diluted PEO solution can be calculated as $[\eta]c\eta_s$, resulting in an expression of $0.072\eta_s cM_w^{0.65}$ according to the above equations. The polymer solution viscosity η can thus be calculated as $\eta_s + 0.072\eta_s cM_w^{0.65}$. The viscosities of 50, 100, 300, and 1200 ppm PEO solutions are also measured by a rheometer (Physica MCR302, Anton Paar GmBH, Germany) with cone-plate geometry (50 mm, 0.017 rad) at 20 ℃ (Fig. 2). For 50-300 ppm PEO solutions, the values of measured shear viscosity are in good agreement with those from the theoretical prediction. With the increased PEO concentration to 1200 ppm, the measured value is ~ 10 % higher than the theoretical value. We should note that the theoretical predication becomes inaccurate when the PEO

View Article Online
DOI: 10.1039/C7LC00671C

concentration is close to the overlap concentration c^* that is 1877 ppm.[30, 36, 37] Elasticity number (*El*), the ratio of *Wi* to *Re*, characterizes the relative importance of flow elasticity to inertia, which is defined as $2\lambda\eta/\rho W^2$. The values of *El*, *Wi*, and *Re* for the present study are listed in Table S1.

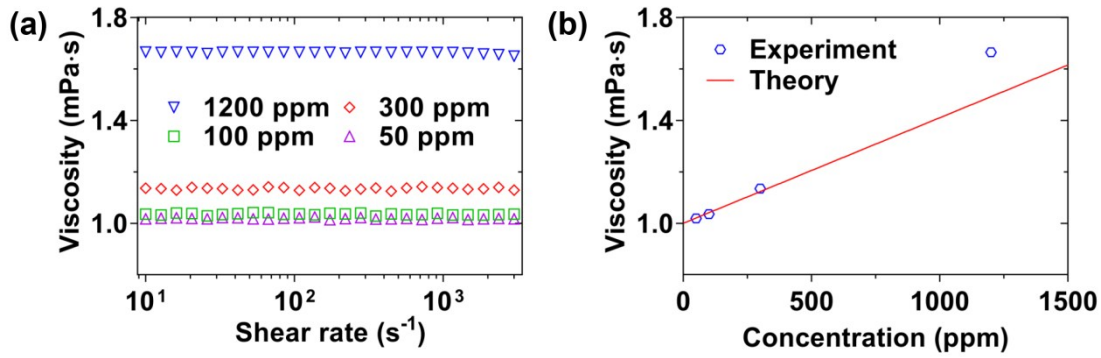

Fig. 2. (a) Shear viscosities of 50, 100, 300, and 1200 ppm PEO solutions measured at 10-3000 s^{-1}. (b) Comparison between the measured and theoretically predicted viscosities.

Results and discussion

Working principle of separation by microfluidic co-flow

Our separation device consists of a straight microchannel with two inlets and five outlets (Fig. 1a). The microparticles-loaded Newtonian fluid (sample flow) and viscoelastic fluid (sheath flow) are introduced into the straight microchannel from the side and central parts, respectively. High Péclet numbers ($Pe = U_{max}W/D_0$, where maximum velocity $U_{max} = 1.42\,m/s$ and $D_0 = 4.45\times10^{-12}\,m^2/s$ is the diffusion coefficient of PEO molecules in water calculated based on the PEO's gyration radius 48 nm[39]) of the order of 10^6 for the present study indicate the diffusion of PEO molecules is negligible. Using a large

View Article Online
DOI: 10.1039/C7LC00671C

sheath/sample flow rate ratio of 8, an interface between the Newtonian and viscoelastic fluids is formed close to the sidewall of straight microchannel (~ 2 μm), which is visualized by spiking fluorescent nanoparticles (100 nm in diameter) into the sheath inlet (Fig. 1b). The separation of microparticles relies on this interface: the penetration of microparticles across the interface from the Newtonian side to viscoelastic side occurs in a size-selective manner (Fig. 1c). Large particles traverse the interface and are collected at the three center outlets, whereas small particles are intercepted by the interface and are collected at the side outlets.

Analytical model of elastic lift forces

We develop an analytical model to quantify the elastic lift forces at the interface. The geometrical variables for the force analysis are depicted in Fig. 3a. A particle with a diameter of a is centered at y_c and the interface is located at y_0. The elastic lift forces acting on the particle are determined by integrating the first normal stress difference N_1 ($N_1 = \tau_{xx} - \tau_{yy}$, where τ is the diagonal component of the stress tensor, and x and y is the directions of the flow and velocity gradient, respectively[40]) over the particle surface portion that immerses in the viscoelastic medium. The N_1 can be expressed as the $N_1 = 2\eta_p \lambda \dot{\gamma}^2$ using Oldroyd-B constitutive model. The low-concentration PEO solution (100 ppm) can be considered as a Boger fluid,[41] where η_p is the polymeric contribution of the solution viscosity, λ is the relaxation time of the PEO solution, $\dot{\gamma}$ is the local shear rate.

View Article Online
DOI: 10.1039/C7LC00671C

$$F_e = \int_0^{\Theta} \sin\theta d\theta \int_0^{2\pi} d\varphi C \left(\frac{a}{2}\right)^2 N_1 \cos\theta$$
$$= \frac{16\pi C a^2 \eta_p \lambda U_{\max}^2}{W^2} \int_0^{\Theta} \sin\theta\cos\theta \left(1 - \frac{2y_c + a\cos\theta}{W}\right)^2 d\theta \quad (1)$$
$$= -\frac{16\pi C a^2 \eta_p \lambda U_{\max}^2 \cos^2\theta}{W^2} \left(\frac{1}{2} + \frac{3a^2\cos^2\theta + 24y_c^2 + 16ay_c\cos\theta - 24Wy_c - 8Wa\cos\theta}{12W^2}\right)\Bigg|_0^{\Theta}$$

where C is the elastic lift coefficient determined as 0.07 from our recently published work,[42] θ is the polar angle of the spherical coordinate system whose origin is located at the particle center, and Θ is the polar angle of the interface and expressed as $\arccos\left[2\left(y_0 - y_c\right)/a\right]$ for particles at the interface. Θ is set as 0 and π when the particle is fully immersed in the Newtonian and viscoelastic fluids, respectively. The solved Eqn. 1 is plotted against y coordinate at y_0 = 2 μm for sheath and sample flow rates of 2.4 and 0.3 mL/h, indicating four distinguishing regimes of the distributions of the elastic lift forces (Fig. 3b dashed lines): (1) $y_c < y_0 - a/2$: the particle is fully immersed in the Newtonian fluid and thus the elastic lift forces are vanishing; (2) $y_0 - a/2 \le y_c \le y_0$: the right side of the particle is at the interface and the elastic lift forces direct toward the sidewalls due to the compressive elastic stresses acting from the center side; (3) $y_0 < y_c \le y_0 + a/2$: the near-wall side of the particle is at the interface and the elastic lift forces become weaker and finally get reversed in direction due to the offset effects of the compressive elastic stresses acting from the near-wall side; and (4) $y_0 + a/2 < y_c \le W/2$: the particle is fully immersed in the viscoelastic fluid and the elastic lift forces direct toward the centerline. We note that the elastic lift forces at the interface are more intensive than the bulk elastic lift forces, allowing particle manipulation using less additive polymer than the case of sheath/sample flows of the same viscoelastic medium.

View Article Online
DOI: 10.1039/C7LC00671C

Force balance between elastic and inertial lift forces

For quantitative analysis, we calculate the force balance of F_L and F_e for particles with a = 1 μm and 2 μm, respectively, at the conditions of Q_v = 2.7 mL/h and c = 100 ppm (Re = 27.2, Wi = 17.4, and El = 0.64). The inertial lift forces are expressed as $F_L = \rho C_L U_{\max}^2 a^4 / W^2$,[6] where C_L is the inertial lift coefficient determined from our previous direct numerical simulation (DNS) (Fig. 3b dashdot lines).[43] For 1 μm particles, the elastic lift forces are stronger than the inertial lift forces at the interface, resulting in a net lift force directed toward the sidewalls. In contrast, the net lift force acting on 2 μm particles are center-directed due to the faster increase of F_L with a than F_e. To clearly present the size-selective particle trap at the interface, we further calculate the potential energy of the net lift force, which is defined as the integration of the net lift force along the y-axis, $\int_{y_c}^{W/2} \left(F_e + F_i\right) dy$ (Fig. 3c). The calculated equilibrium positions reveal an efficient separation of 1 μm and 2 μm particles. 1 μm particles are trapped at the interface whereas 2 μm particles penetrate the interface and are finally focused at the midway of the sidewalls and the centerline, forming into two side streaks instead of a single central streak, which is similar to the multi-train focusing observed by Xiang *et al*..[44] Side streaks usually appear when the fluid inertial effect is comparable with the elastic effect (El is of the order of 1),[44] while our analysis also indicates that the magnitudes of inertial and elastic lift forces are of the same order under the El of 0.64 (Fig. 3b).

View Article Online
DOI: 10.1039/C7LC00671C

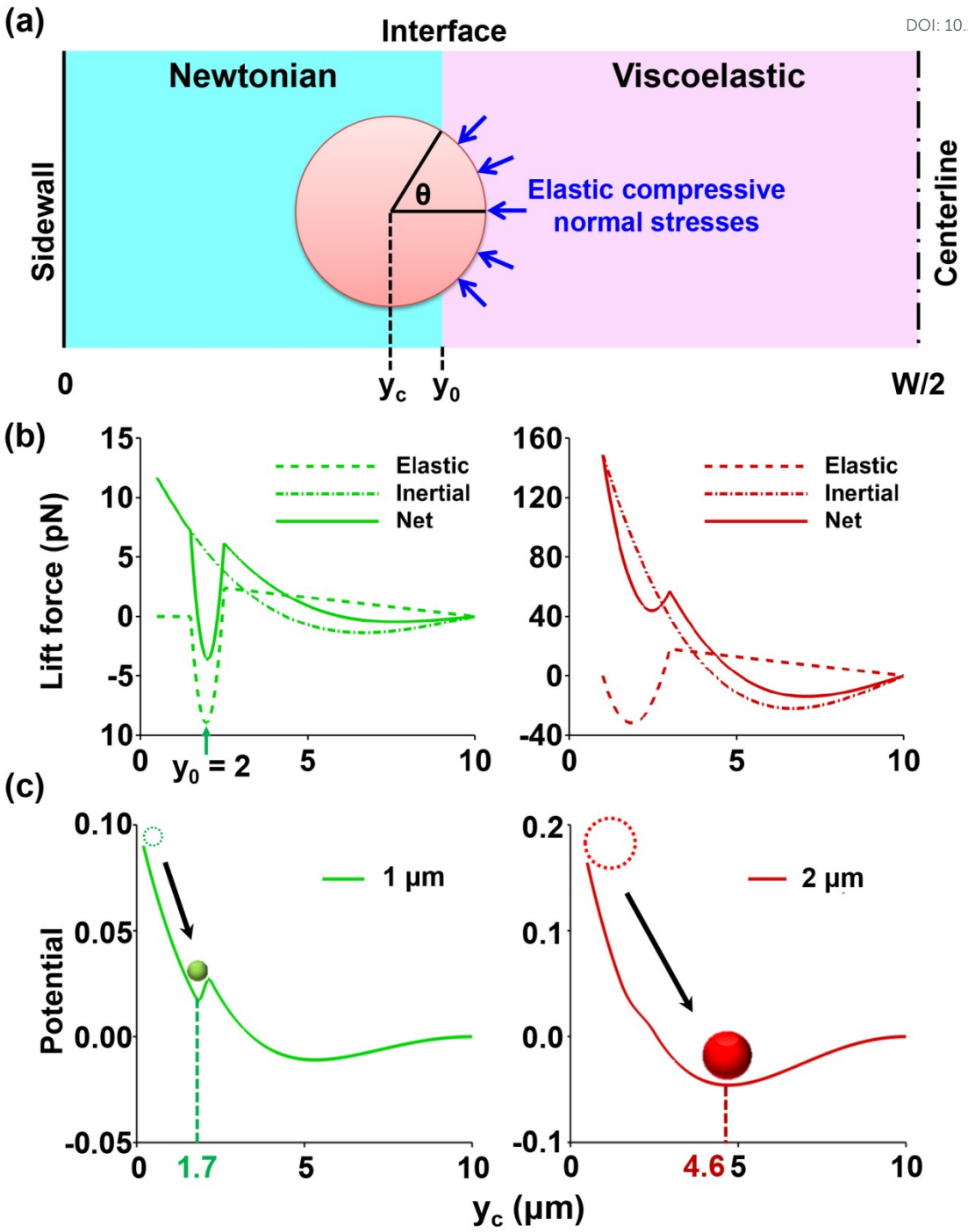

Fig. 3. (a) Schematic of a spherical particle migrating across the Newtonian-viscoelastic interface. (b) The values of elastic lift forces (dash), inertial lift forces (dashdot), and net lift forces (solid) and (c) the potential of the net lift forces plotted at different lateral positions (y) for 1 μm (green) and 2 μm (red) particles, respectively. Positive and negative force values represent center-directed and wall-directed forces, respectively. The microchannel sidewall

View Article Online
DOI: 10.1039/C7LC00671C

and centerline are located at y = 0 μm and 10 μm, respectively. The lateral position of the interface y_0 is 2 μm for sheath and sample flow rates of 2.4 and 0.3 mL/h. The potential is normalized by $0.5m_pU_{\max}^2$.

Microparticle separation

The separation performance is validated using a mixture of PS particles with a of 1 μm (green) and 2 μm (red) for three sheath/sample flow conditions: viscoelastic/Newtonian (vis/N), viscoelastic/viscoelastic (vis/vis), and Newtonian/Newtonian (N/N) (Fig. 4). The particle concentrations are 0.02 % and 0.2 % for 1 μm and 2 μm particles, corresponding to a number ratio of 1 to 1.25. The sheath and sample flow rates are 2.4 and 0.3 mL/h, respectively. The particle distributions are shown in standard deviation plots from 1000 image stacks at the different downstream locations. In the vis/N condition, the initially randomly distributed particles are completely separated at the microchannel outlet. The 1 μm particles blocked by the interface remain near the sidewalls and exit through the side outlets, whereas 2 μm particles penetrate the interface, and are collected from the three center outlets. Without the block effect of the interface, 1 μm particles in the vis/vis condition migrate closer toward the microchannel centerline compared with the vis/N condition, while 2 μm particles reach similar lateral positions compared with the vis/N condition due to the same lift force distribution in the sheath fluid. In the N/N condition, both 1 μm and 2 μm particles have the similar equilibrium positions at 0.6 times of the half channel width away from the centerline under the pure inertial focusing effect, resulting in almost no separation between these two particle populations. Therefore, the vis/N condition yields a much larger separation distance

View Article Online
DOI: 10.1039/C7LC00671C

between 1 μm and 2 μm particles than that for the vis/vis and N/N conditions. Based on this large separation distance, the separation efficiency and purity for 1 μm and 2 μm particles in the vis/N condition both reach ~ 100 %. In contrast, the separation efficiency and purity suffer serious decrease under the vis/vis and N/N conditions.

View Article Online
DOI: 10.1039/C7LC00671C

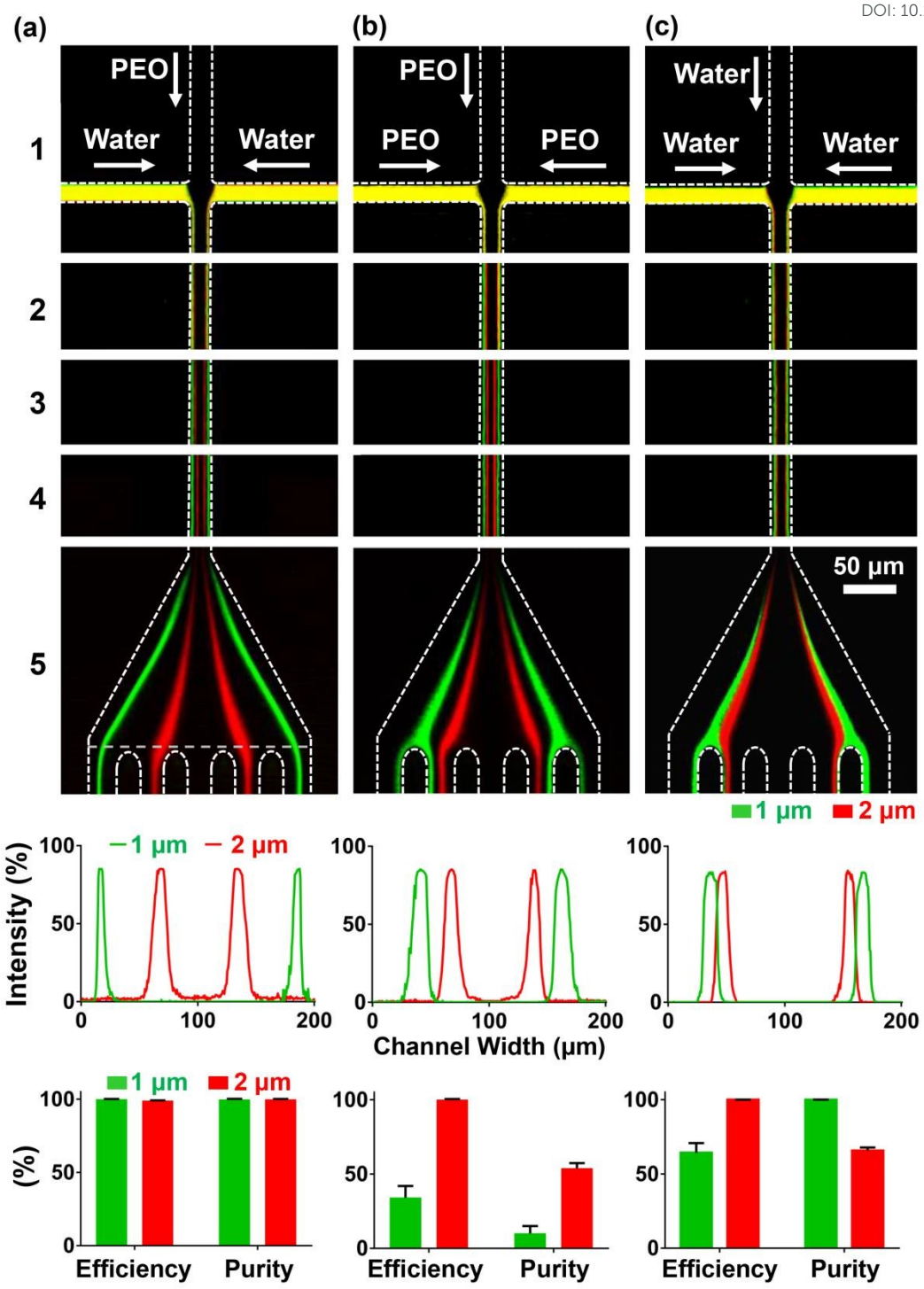

Fig. 4. Experimental observation of separation of particles with different sizes. The separation of a mixture of 1 μm (green) and 2 μm (red) particles is performed under three sheath/sample flow conditions: (a) viscoelastic/Newtonian, (b) viscoelastic/viscoelastic, and (c) Newtonian/Newtonian, in terms of particle trajectories (top), fluorescent intensities

View Article Online
DOI: 10.1039/C7LC00671C

(middle), and efficiencies and purities (bottom). The sheath and sample flow rates 2.4 and 0.3 mL/h, respectively. The viscoelastic medium is 100 ppm PEO solution.

Effects of PEO concentration and flow rate

The PEO concentration c of the sheath fluid has complex effects on the particle separation performance. As the relaxation time of the PEO solution increases with $c^{1.65}$, increasing c can enhance the wall-directed interfacial elastic lift forces. Larger particle size is then required to penetrate the interface at higher c, resulting in a lower size resolution for particle separation. On the other hand, increasing c can lead to the further migration toward the microchannel centerline once the large particles penetrate the interface, thus enhancing the separation distance. To determine an optimal c for best separation performance, we should consider the balance between the above two factors. The separation performance of 1 μm and 2 μm particles at various c ranging from 50 to 1200 ppm is systemically evaluated (Fig. 5). The particle trajectories at the outlet show that using only 50 ppm PEO sheath fluid, the interfacial elastic lift forces are sufficiently strong to trap 1 μm particles, whereas 2 μm particles penetrate the interface and reach equilibrium positions in the sheath fluid (Fig. 5a). Increasing c to 100 ppm, 1 μm particles are still trapped at the interface as expected, while the equilibrium positions of 2 μm particles shift toward the microchannel centerline due to the enhanced elastic lift forces, resulting in a larger separation distance. However, increasing c to 300 ppm, a part of 2 μm particles are trapped at the interfaces, since the interfacial elastic lift forces begin to dominate over the wall repulsion. At c = 1200 ppm, all 2 μm particles are trapped at the interface, leading to no separation. The separation efficiencies (Fig. 5b) and

View Article Online
DOI: 10.1039/C7LC00671C

purities (Fig. 5c) suggest that the best separation performance is obtained at c = 100 ppm, which is consistent with the particle trajectory observations. The separation performance is less sensitive to the flow rate than PEO concentration probably because both elastic and inertial lift forces are proportional to $U_{\max}^2$. The separation efficiencies and purities of 1 μm and 2 μm particles are calculated at various sheath flow rates ranging from 1.2 to 3.0 mL/h with a fixed sample flow rate of 0.3 mL/h (Table 1). Both the separation efficiencies and purities maintain a consistent value > 98 % at sheath flow rates from 1.8 to 3.0 mL/h. The reduced performance at the sheath flow rate of 1.2 mL/h is probably due to the dispersed sample input at low sheath/sample ratio of 4.

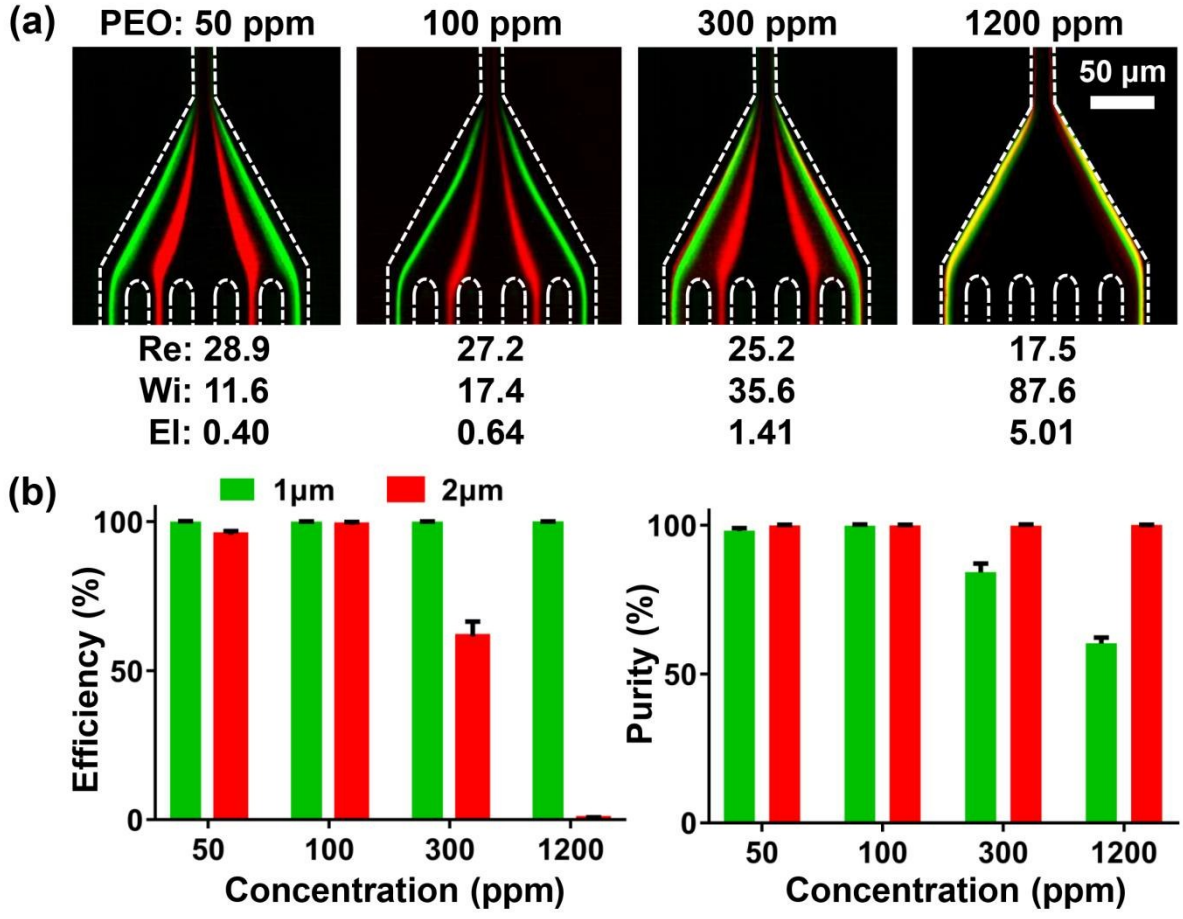

View Article Online
DOI: 10.1039/C7LC00671C

Fig. 5. (a) Particle trajectories at the outlet and (b) separation efficiencies and purities of 1 μm (green) and 2 μm (red) at different PEO concentrations from 50 to 1200 ppm. The sheath and sample flow rates are at 2.4 and 0.3 mL/h, respectively.

Table 1 Separation efficiencies and purities of 1 μm and 2 μm at various sheath flow rates ranging from 1.2 to 3.0 mL/h with a fixed sample flow rate of 0.3 mL/h. The PEO concentration is 100 ppm for the sheath medium.

Sheath flow rate (mL/h)	**Efficiency (%)**		**Purity (%)**	
	1 μm	2 μm	1 μm	2 μm
1.2	64.35 ±4.15	86.67 ±5.41	94.63 ±2.21	46.91 ±3.74
1.8	96.53 ±0.80	96.35 ±1.20	97.97 ±0.87	93.91 ±0.61
2.4	99.87 ±0.23	98.96 ±0.96	99.74 ±0.46	99.80 ±0.35
3.0	99.78 ±0.15	98.89 ±0.83	99.69 ±0.57	99.78 ±0.39

Separation of bacteria from platelets

The separation of small-sized bio-particles, such as platelets and bacteria, is important in apheresis platelet safety and hematological immunity investigation.[45, 46] Based on the successful separation of the binary mixture of 1 μm and 2 μm PS particles, we further apply the present technique to separation SA (1 μm) and platelets (2-3 μm). The samples are prepared by adding SA into 4× diluted platelets. The volumetric fraction of total cells is controlled to be 0.1 % to minimize the cell-cell interaction. The cell experiments are run under the same conditions as for the PS particles, except for using PBS buffer instead of DI water. The stacked image of the trajectories of SA and platelets at the outlets indicates a

View Article Online
DOI: 10.1039/C7LC00671C

complete separation of SA and platelets, while SA and platelets exhibit almost the same focusing equilibrium positions compared with 1 μm and 2 μm PS particles (Fig. 6). A bright-field movie is available in the Supplementary Information. The separation efficiencies of SA and platelets are determined as 97 % and 100 %, respectively.

We note that most of previous works on viscoelastic particle separation are performed in elastic flows with $El >> 1$ (Table S2). In the present study, the separation of microparticles and cells smaller than 3 μm can be obtained at *El* less than the unity. With comparable channel dimensions to previous works, the low *El* is attributed to the short λ and low η of dilute (50-100 ppm) PEO solutions used for the separation. The elastic lift force is more intensive at the interface compared with that in viscoelastic fluid body due to the absence of offset elastic stresses from the Newtonian side, allowing for the efficient particle separation at low polymer concentrations.

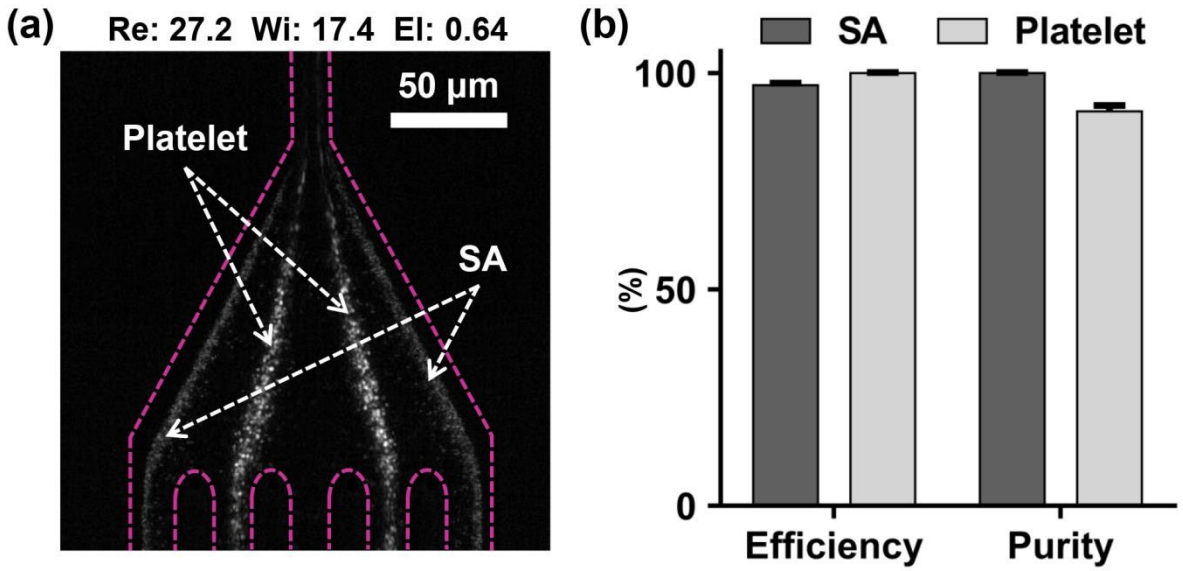

Fig. 6. Complete separation of the mixture of SA and Platelet. (a) The stacked image of

View Article Online
DOI: 10.1039/C7LC00671C

trajectories of SA and platelet at the outlet. (b) The separation efficiencies and purities of SA and platelet. The sheath and sample flow rates are 2.4 and 0.3 mL/h, respectively. The viscoelastic medium is 100 ppm PEO solution.

Conclusion

In this work, we present a label-free, high-efficient, and high-resolution separation technique for processing particles, bacteria, and platelets smaller than 3 μm, based on the size-dependent penetration of the viscoelastic/Newtonian interface inside a co-flow microfluidic device. Compared with existing hydrodynamic separation techniques using single-phase Newtonian or viscoelastic flow conditions, the co-flow condition generates a stable viscoelastic/Newtonian interface, giving rise to the wall-directed interfacial elastic lift forces that compete with the center-directed inertial lift forces. The interaction between two forces results in a large separation distance between different size particles, yielding the high separation efficiency and purity ~ 100 %. Moreover, the polymer concentration used in the co-flow set-up is much lower than that in pure viscoelastic condition, attributed to the much intensive interfacial elastic lift forces than the bulk elastic lift forces. The low concentration of PEO provides a more suitable condition for manipulation of bio-samples. This separation technique may become a promising tool for processing small bio-particles of similar sizes.

Acknowledgements

This work was supported financially by NSFC (21622503, 21475028, 11572334), Youth Innovation Promotion Association CAS (2016035), Beijing Municipal Science and

View Article Online
DOI: 10.1039/C7LC00671C

Technology Commission (Z171100001117135, Z161100004916095), Joint Doctoral Training Foundation of HEBUT, Hebei in Graduate Student Innovation Ability Training Project.

References

1. J. C. Giddings, *Science*, 1993, **260**, 1456-1465.
2. M. Toner and D. Irimia, *Annu. Rev. Biomed. Eng.*, 2005, **7**, 77-103.
3. X. Ding, Z. Peng, S.-C. S. Lin, M. Geri, S. Li, P. Li, Y. Chen, M. Dao, S. Suresh and T. J. Huang, *Proc. Natl. Acad. Sci. U. S. A.*, 2014, **111**, 12992-12997.
4. D. Di Carlo, J. Edd, K. Humphry, H. Stone and M. Toner, *Phys. Rev. Lett.*, 2009, **102**, 094503.
5. A. M. Leshansky, A. Bransky, N. Korin and U. Dinnar, *Phys. Rev. Lett.*, 2007, **98**, 234501.
6. B. P. Ho and L. G. Leal, *J. Fluid Mech.*, 1974, **65**, 365-400.
7. B. P. Ho and L. G. Leal, *J. Fluid Mech.*, 1976, **76**, 783-799.
8. G. Segre and A. Silberberg, *Nature*, 1961, **189**, 209-210.
9. J.-P. Matas, J. F. Morris and É. Guazzelli, *J. Fluid Mech.*, 2004, **515**, 171-195.
10. D. Di Carlo, D. Irimia, R. G. Tompkins and M. Toner, *Proc. Natl. Acad. Sci. U. S. A.*, 2007, **104**, 18892-18897.
11. A. A. S. Bhagat, S. S. Kuntaegowdanahalli and I. Papautsky, *Phys. Fluids*, 2008, **20**, 101702.
12. S. C. Hur, H. T. K. Tse and D. Di Carlo, *Lab Chip*, 2010, **10**, 274-280.
13. C. Liu, G. Hu, X. Jiang and J. Sun, *Lab Chip*, 2015, **15**, 1168-1177.
14. M. G. Lee, S. Choi and J. K. Park, *J. Chromatogr. A*, 2011, **1218**, 4138-4143.
15. A. J. Chung, D. Pulido, J. C. Oka, H. Amini, M. Masaeli and D. Di Carlo, *Lab Chip*, 2013, **13**, 2942-2949.
16. X. Lu and X. Xuan, *Anal. Chem.*, 2015, **87**, 4560-4565.
17. Z. Wu, Y. Chen, M. Wang and A. J. Chung, *Lab Chip*, 2016, **16**, 532-542.
18. H. W. Hou, M. E. Warkiani, B. L. Khoo, Z. R. Li, R. A. Soo, D. S.-W. Tan, W.-T. Lim, J. Han, A. A. S. Bhagat and C. T. Lim, *Sci. Rep.*, 2013, **3**, 1259.
19. J. Zhang, S. Yan, R. Sluyter, W. Li, G. Alici and N.-T. Nguyen, *Sci. Rep.*, 2014, **4**, 4527.
20. N. Xiang, K. Chen, D. Sun, S. Wang, H. Yi and Z. Ni, *Microfluid. Nanofluid.*, 2013, **14**, 89-99.
21. N. Xiang, K. Chen, Q. Dai, D. Jiang, D. Sun and Z. Ni, *Microfluid. Nanofluid.*, 2015, **18**, 29-39.
22. G. D'Avino, G. Romeo, M. M. Villone, F. Greco, P. A. Netti and P. L. Maffettone, *Lab Chip*, 2012, **12**, 1638-1645.
23. K. Kang, S. S. Lee, K. Hyun, S. J. Lee and J. M. Kim, *Nat. Commun.*, 2013, **4**, 2567.
24. E. J. Lim, T. J. Ober, J. F. Edd, S. P. Desai, D. Neal, K. W. Bong, P. S. Doyle, G. H. McKinley and M. Toner, *Nat. Commun.*, 2014, **5**, 4120.

25. J. Nam, H. Lim, D. Kim, H. Jung and S. Shin, *Lab Chip*, 2012, **12**, 1347-1354.
26. F. Del Giudice, G. Romeo, G. D'Avino, F. Greco, P. A. Netti and P. L. Maffettone, *Lab Chip*, 2013, **13**, 4263-4271.
27. C. Liu, C. Xue, X. Chen, L. Shan, Y. Tian and G. Hu, *Anal. Chem.*, 2015, **87**, 6041-6048.
28. S. Yang, S. S. Lee, S. W. Ahn, K. Kang, W. Shim, G. Lee, K. Hyun and J. M. Kim, *Soft Matter*, 2012, **8**, 5011-5019.
29. D. Yuan, J. Zhang, R. Sluyter, Q. Zhao, S. Yan, G. Alici and W. Li, *Lab Chip*, 2016, **16**, 3919-3928.
30. C. Liu, B. Ding, C. Xue, Y. Tian, G. Hu and J. Sun, *Anal. Chem.*, 2016, **88**, 12547-12553.
31. X. Lu and X. Xuan, *Anal. Chem.*, 2015, **87**, 6389-6396.
32. X. Lu and X. Xuan, *Anal. Chem.*, 2015, **87**, 11523-11530.
33. D. Yuan, J. Zhang, S. Yan, G. Peng, Q. Zhao, G. Alici, H. Du and W. Li, *Electrophoresis*, 2016, **37**, 2147-2155.
34. B. Ha, J. Park, G. Destgeer, J. H. Jung and H. J. Sung, *Anal. Chem.*, 2016, **88**, 4205-4210.
35. G. F. Guan, L. D. Wu, A. A. S. Bhagat, Z. R. Li, P. C. Y. Chen, S. Z. Chao, C. J. Ong and J. Y. Han, *Sci. Rep.*, 2013, **3**, 1475.
36. V. Tirtaatmadja, G. H. McKinley and J. J. Cooper-White, *Phys. Fluids*, 2006, **18**, 043101.
37. W. W. Graessley, *Polymer*, 1980, **21**, 258-262.
38. L. E. Rodd, T. P. Scott, D. V. Boger, J. J. Cooper-White and G. H. McKinley, *J. Non-Newton. Fluid Mech.*, 2005, **129**, 1-22.
39. K. Devanand and J. C. Selser, *Macromolecules*, 1991, **24**, 5943-5947.
40. H. A. Barnes, J. F. Hutton and K. Walters, *An introduction to rheology*, Elsevier, Amsterdam, 1989.
41. D. F. James, *Annu. Rev. Fluid Mech.*, 2009, **41**, 129-142.
42. C. Liu, J. Guo, F. Tian, N. Yang, F. Yan, Y. Ding, J. Wei, G. Hu, G. Nie and J. Sun, *ACS Nano*, 2017, DOI: 10.1021/acsnano.7b02277.
43. C. Liu, C. Xue, J. Sun and G. Hu, *Lab Chip*, 2016, **16**, 884-892.
44. N. Xiang, Q. Dai and Z. Ni, *Appl. Phys. Lett.*, 2016, **109**, 134101.
45. M. A. Blajchman, M. Goldman and F. Baeza, *Transf. Med. Rev.*, 2004, **18**, 11-24.
46. J. R. Fitzgerald, T. J. Foster and D. Cox, *Nat. Rev. Microbiol.*, 2006, **4**, 445-457.